Nematic Equilibria on a Two-Dimensional Annulus

By A. H. Lewis, D. G. A. L. Aarts, P. D. Howell, and A. Majumdar

We study planar nematic equilibria on a two-dimensional annulus with strong and weak tangent anchoring, in the Oseen–Frank theoretical framework. We analyze a radially invariant defect-free state and compute analytic stability criteria for this state in terms of the elastic anisotropy, annular aspect ratio, and anchoring strength. In the strong anchoring case, we define and characterize a new spiral-like equilibrium which emerges as the defect-free state loses stability. In the weak anchoring case, we compute stability diagrams that quantify the response of the defect-free state to radial and azimuthal perturbations. We study sector equilibria on sectors of an annulus, including the effects of weak anchoring and elastic anisotropy, giving novel insights into the correlation between preferred numbers of boundary defects and the geometry. We numerically demonstrate that these sector configurations can approximate experimentally observed equilibria with boundary defects.

1. Introduction

Nematic liquid crystals (LCs) are classic examples of partially ordered materials that combine the fluidity of liquids with the orientational order of crystalline solids [1, 2]. Nematics have generated substantial scientific interest in recent years because of their unique optical, mechanical, and rheological properties [3] and, notably, nematics form the backbone of the multibillion dollar liquid crystal display (LCD) industry. Defects are a key feature of nematic spatiotemporal patterns in confined geometries. Much

Address for correspondence: Dr. A. Majumdar, Department of Mathematical Sciences, University of Bath, Bath BA2 7AY, UK; e-mail: a.majumdar@bath.ac.uk

DOI: 10.1111/sapm.12161

STUDIES IN APPLIED MATHEMATICS 138:438–466

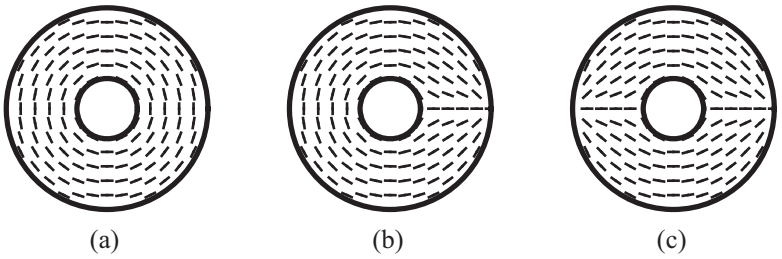

Figure 1. Nematic director fields identified experimentally in [4, 5]: (a) defect-free state; (b) one defect on each boundary; and (c) two defects on each boundary.

remains to be understood about the structure of defects and how they can be created, controlled, and manipulated to yield desired properties.

In this paper, we revisit the classical problem of a nematic sample in a two-dimensional (2D) annulus with strong or weak tangent boundary conditions and no external fields. Our work is motivated in part by recent experiments [4–6] on rod-like *fd*-virus particles within shallow, annular microscopic chambers. The experiments exhibit at least six different stable states, including a radially invariant defect-free state, and states with regularly arranged defects on the boundary; for example, see Fig. 1. This paper is devoted to an analytical and numerical study of the defect-free state and states with pinned boundary defects using the Oseen–Frank (OF) theory for LCs. Our aim is to understand why a state with boundary defects might be observed and in which situations it could be energetically preferable to have boundary defects.

The model problem of a defect-free state in an annular well has received a great deal of attention in the past, especially within OF theory. Here, we give a brief overview. The papers [7–14] are directly relevant to our work. In Ref. [8], the author studies the stability and multiplicity of nematic radial equilibria on a 2D annulus with strong uniform anchoring. In Refs. [9–12], the authors approach the same problem with a more applications-oriented perspective motivated by the classical Fréederickzs transition. They study confined nematic samples between two concentric cylinders with weak anchoring on one lateral surface and strong anchoring on another, subject to an external magnetic field. The authors primarily consider the stability of three characteristic configurations, referred to as "radial," "azimuthal," and "uniform," and obtain explicit estimates for the critical threshold field in terms of the OF elastic anisotropy, cylindrical aspect ratio, and anchoring strength. An analogous problem was studied in [14] for the case of strong axial anchoring. Finally, in Ref. [7], the authors demonstrate that the planar radial state loses stability when the ratio of the inner radius to the outer radius is smaller than a critical value, and the planar radial state

escapes into the third dimension. In Ref. [13], the authors study nematic samples confined between two coaxial cylinders, with emphasis on higher dimensional biaxial effects, which are outside the scope of the present paper.

We build on this extensive body of work in the OF theoretical framework. We study the defect-free state with strong tangential anchoring prescribed in terms of Dirichlet conditions and with weak tangential anchoring described by a surface energy. The defect-free state in our paper is analogous to the azimuthal state on an annulus, with tangent boundary conditions on both circular boundaries [9–12]. The three key parameters are the elastic anisotropy (δ), the annular aspect ratio (ρ), and the anchoring strength (α). In the strong anchoring case, we characterize a new spiral-like equilibrium that emerges from the defect-free state, as it loses stability with increasing δ. In the weak anchoring case, we analyze the defect-free state in terms of δ, ρ, α, and k, which is the azimuthal order of the perturbation. While our results, both with strong and weak anchoring, are partially captured by the results in [8–12], our method of proof is different. By computing the second variation of the anisotropic OF energy and studying the resulting eigenvalue problem directly, we obtain new stability diagrams for the defect-free state in terms of δ, ρ, α, and k. Such stability diagrams can provide useful insight into the response of the defect-free state to different types of azimuthal perturbations. For $k = 0$, our results reduce to the previously reported results in [8–12]. An interesting conclusion is that the radially invariant defect-free state can largely be destabilized by radial perturbations and azimuthal perturbations are only relevant for weak anchoring or very small annular wells.

The second part of this paper focuses on an analytic description of experimentally observed equilibria with boundary defects. Our modeling approach is to partition the annulus into sectors, construct "sector configurations" which naturally have defects at the sector vertices, and finally glue the sector configurations along the common edges to generate an approximate equilibrium configuration on the whole annulus. In particular, we focus on generalized "rotated" and "diagonal" solutions in a sector, by analogy with parallel work on rectangular wells in [15, 16]. We compare the energies of these sector-based equilibria with that of the defect-free state, including effects of weak anchoring and elastic anisotropy. Our idealized model suggests that it may be energetically preferable to have boundary defects either for large δ or for moderate values of α, but never with $\delta = 0$ (elastic isotropy) and strong anchoring. This conclusion agrees with experimental observations.

Since it is not clear *a priori* whether real-life equilibria respect the symmetries implicit in our sector-based equilibria, we also compare our results with computations of a numerical gradient-flow scheme for a 2D Landau-de Gennes (LdG)-type energy with weak anchoring. We use the

sector configurations to construct initial conditions and find that the long-time dynamics respects the symmetries of the initial condition, and the overall structure is qualitatively similar to the sector-based equilibrium, at least for the certain choices of parameter values. We conclude that our sector configurations do mimic real equilibria in certain situations at least.

Equilibria with boundary defects can be interesting in many physical situations, particularly with Neumann boundary conditions or when we simply specify topological degrees on the boundaries, as opposed to Dirichlet conditions. For example, in [17], the authors study 2D vector fields, $\mathbf{u} = (u_1, u_2)$, on a multiply connected 2D domain with prescribed topological degrees on the outer boundary and on the inner boundaries enclosing the "holes." The authors study minimizers of the Ginzburg–Landau functional on such domains and find that the infimum energy is not attained. Minimizing sequences develop vortices or boundary defects in certain asymptotic limits. Our construction for equilibria with boundary defects could be instructive for such model LC problems, with topological degree boundary conditions; in fact, they give information about minimizing sequences. Equally importantly, our analysis is directly relevant to recent experimental work on colloidal samples in shallow annular wells wherein the authors observe states with defects pinned to the lateral surfaces [4, 5], such as those shown in Figs. 1(b) and (c). The relative energies of the generalized "diagonal" and "rotated" states give qualitative insight into the relative observational frequencies of the experimental states that exhibit boundary defects.

The paper is organized as follows. In Section 2, we review the OF theory for nematic LCs, and use it to formulate the problem and boundary conditions. In Section 3, we compute stability criteria for the defect-free state as a function of δ, ρ, and α as introduced above. In Section 4, we construct sector-based equilibria on an annulus with an arbitrary number of boundary defects and compute the corresponding energies. Finally, we discuss our results and draw conclusions in Section 5.

2. Theory and modeling

We study nematic equilibria on a 2D annulus, subject to tangent boundary conditions. The rescaled 2D annulus is defined by

$$\Omega = \{(r, \phi) \in \mathbb{R}^2 : \quad \rho \leq r \leq 1, \quad 0 \leq \phi < 2\pi\}, \tag{1}$$

where $\rho := R_{\text{inner}}/R_{\text{outer}}$ is the ratio of the inner and outer radii.

We work in the simplest OF framework, restricted to a uniaxial nematic phase with a constant scalar order parameter [1, 2]. In this case, the macroscopic order parameter is simply a unit-vector field, $\mathbf{n}$, that defines the

unique direction of preferred molecular alignment. For a 2D problem, the OF energy functional is given by

$$E[\mathbf{n}] := \int_\Omega \frac{K_1}{2}(\nabla \cdot \mathbf{n})^2 + \frac{K_3}{2}\big(\mathbf{n} \times (\nabla \times \mathbf{n})\big)^2 \, \mathrm{d}\Omega, \tag{2}$$

where K_1 and K_3 are the elastic constants associated with splay and bend deformations, respectively. The twist constant is neglected because $\mathbf{n} \cdot \nabla \times \mathbf{n} = 0$ for a 2D vector field. Similarly, the saddle-splay term, $(K_2 + K_4)\nabla \cdot ((\nabla \times \mathbf{n}) \times \mathbf{n} - (\nabla \cdot \mathbf{n})\mathbf{n})$ is also identically zero for 2D vector fields. In three dimensions, for Dirichlet boundary conditions, this saddle-splay term is a fixed energetic contribution and hence, can be neglected. For weak anchoring, this term can matter since it is effectively a surface energy.

For 2D deformations, the director is parameterized by $\mathbf{n} = (\cos\theta, \sin\theta, 0)$, where $\theta : \Omega \to \mathbb{R}$ is a function of the planar polar co-ordinates, (r, ϕ). The OF energy (2), normalized with K_3, then reduces to

$$\begin{aligned} E[\theta] := \int_\Omega \frac{1-\delta}{2}\left(\cos(\theta-\phi)\frac{\theta_\phi}{r} - \sin(\theta-\phi)\theta_r\right)^2 \\ + \frac{1}{2}\left(\sin(\theta-\phi)\frac{\theta_\phi}{r} + \cos(\theta-\phi)\theta_r\right)^2 \mathrm{d}\Omega, \end{aligned} \tag{3}$$

where $\delta := 1 - K_1/K_3$ is the measure of elastic anisotropy, so that $\delta = 0$ in the commonly used isotropic "one-constant" approximation. The Euler–Lagrange equation corresponding to critical points of (3) may be written in the form

$$\begin{aligned} \left(1 - \frac{\delta}{2}\right)\nabla^2\theta + \frac{\delta}{2}\Bigg[\sin(2\theta - 2\phi)\left(\frac{2\theta_{r\phi}}{r} + \frac{\theta_\phi^2}{r^2} - \theta_r^2 - \frac{2\theta_\phi}{r^2}\right) \\ + \cos(2\theta - 2\phi)\left(\theta_{rr} - \frac{\theta_{\phi\phi}}{r^2} - \frac{\theta_r}{r} + \frac{2\theta_r\theta_\phi}{r}\right)\Bigg] = 0 \end{aligned} \tag{4}$$

subject to appropriate boundary conditions for θ on $\partial\Omega$.

We work with both strong and weak boundary conditions in the OF framework. The strong boundary conditions are equivalent to Dirichlet conditions for θ on $r = \rho$ and $r = 1$, namely,

$$\theta(1, \phi) = \phi + \left(n + \frac{1}{2}\right)\pi, \qquad \theta(\rho, \phi) = \phi + \left(m + \frac{1}{2}\right)\pi, \tag{5}$$

where $n, m \in \mathbb{Z}$. Weak anchoring models the tangent boundary conditions by means of a surface energy. We employ the popular Rapini–Papoular surface

energy [18], which in normalized form reads as

$$E_S = \frac{1}{2}\int_{\partial\Omega} \alpha \cos^2(\theta - \phi)\, \mathrm{d}\sigma, \tag{6}$$

where $\partial\Omega$ consists of two concentric circles, with radii $r = \rho$ and $r = 1$, and $\mathrm{d}\sigma$ is arc-length element along $\partial\Omega$. The dimensionless anchoring strength $\alpha := R_{\text{outer}}/\xi$ is the ratio of the outer radius to the extrapolation length ξ, [16], and the three key modeling parameters are then δ, ρ, and α. The extrapolation length, $\xi = K_3/W$, is the ratio of the bending elastic constant to the physical surface anchoring strength parameter W, such that $W \to \infty$ describes the strong anchoring regime [16]. The boundary conditions corresponding to (6) are

$$(2-\delta)\,\theta_r + \delta\left(\frac{\theta_\phi}{r}\sin(2\theta - 2\phi) + \theta_r \cos(2\theta - 2\phi)\right) - \alpha \sin(2\theta - 2\phi) = 0 \quad \text{on} \quad r = 1, \tag{7}$$

$$(2-\delta)\,\theta_r + \delta\left(\frac{\theta_\phi}{r}\sin(2\theta - 2\phi) + \theta_r \cos(2\theta - 2\phi)\right) + \alpha \sin(2\theta - 2\phi) = 0 \quad \text{on} \quad r = \rho. \tag{8}$$

3. The defect-free state in OF theory

3.1. The defect-free state

In the OF framework, the 2D director field is characterized by a single scalar field, namely, the angle $\theta(r, \phi)$, which satisfies the nonlinear elliptic partial differential equation (4). This relatively simple mathematical framework allows us to find explicit sharp stability bounds, and also to describe the behavior of the director when the defect-free state loses stability, as shown below. We define the radially invariant defect-free state to be

$$\theta\,(r, \phi) = \theta^*(\phi) := \phi + \frac{\pi}{2}, \tag{9}$$

which satisfies both the Dirichlet boundary conditions (5) associated with strong anchoring and the nonlinear boundary conditions (7)–(8) associated with weak anchoring. In both cases, we analyze the stability of the defect-free state (9) by studying the second variation of the OF energy, obtain sharp conditions on the model parameters for the defect-free state to be stable, and analyze the bifurcation behavior at the onset of instability.

3.2. Strong anchoring

For strong anchoring defined by (5), we define perturbations $\theta(r,\phi) = \theta^*(\phi) + \epsilon\eta(r,\phi)$, where $\eta(\rho,\phi) = \eta(1,\phi) = 0$. A straightforward computation shows that the second variation is given by

$$\delta^2 E := \left.\frac{\partial^2 E[\theta^* + \epsilon\eta]}{\partial\epsilon^2}\right|_{\epsilon=0} = \int_\Omega (\nabla\eta)^2 - \delta\left(\frac{\eta}{r} + \eta_r\right)^2 \mathrm{d}\Omega$$
$$= E_2\big(\eta(r);\delta,\rho\big). \tag{10}$$

It follows immediately that $\delta^2 E > 0$ for $\delta \le 0$ and any nontrivial η. Local stability is guaranteed by the positivity of the second variation for all admissible perturbations and the defect-free state is unstable if we can find a perturbation η for which E_2 above is negative [19]. On the other hand, let $\delta = 1$ and consider a perturbation $\eta(r)$ whereby the second variation (10) simplifies to

$$E_2\big(\eta(r);1,\rho\big) = -2\pi\int_\rho^1 \frac{\eta^2}{r} + 2\eta\eta_r\,\mathrm{d}r = -2\pi\int_\rho^1 \frac{\eta^2}{r}\,\mathrm{d}r < 0 \tag{11}$$

for nontrivial $\eta(r)$. We can therefore use the continuity of E_2 with respect to δ to deduce that the defect-free state loses stability when $\delta > \delta_c$ for some $\delta_c \in (0,1)$.

We analyze the loss of stability in more detail by studying the Sturm–Liouville problem associated with the minimization of $\delta^2 E$ as shown below. The Euler–Lagrange equation corresponding to (10) is

$$(1-\delta)\left(\eta_{rr} + \frac{\eta_r}{r}\right) + \frac{\eta_{\phi\phi}}{r^2} + \frac{\delta\eta}{r^2} = 0, \tag{12}$$

where $\eta = 0$ on $r = \rho$, 1 and η is 2π-periodic in ϕ. Without loss of generality, we consider separable solutions of the form $\eta(r,\phi) = \sum_{k=0}^{\infty} \mathrm{e}^{\mathrm{i}k\phi} f_k(r)$, where the function $f_k(r)$ is a solution of

$$r^2 f_k''(r) + r f_k'(r) + \frac{\delta - k^2}{1-\delta} f_k(r) = 0, \qquad f_k(\rho) = f_k(1) = 0. \tag{13}$$

Nontrivial solutions $f_k(r)$ exist only for specific values of $\delta = \delta_1, \delta_2, \cdots$, and alternative solution branches bifurcate from the base state θ^* as δ crosses each of these values.

For $k \ge 1$ and $\delta \in (0,1)$, the problem (13) admits no nontrivial solutions. We therefore focus on the case $k = 0$, for which nontrivial solutions of (13) are given by

$$f_{0,n}(r) = A\sin\left(\pi n\,\frac{\log(r)}{\log(\rho)}\right), \qquad \delta_n = \frac{\pi^2 n^2}{\pi^2 n^2 + \log(\rho)^2}, \tag{14}$$

where $n = 1, 2, \cdots$. Since $0 < \delta_1 < \delta_2 < \cdots < 1$, the smallest value of δ yielding nontrivial solutions to (13) is δ_1. Substituting (14) into (10) with $n = 1$, we find that $\delta^2 E < 0$ for $\delta > \delta_1$. Therefore, as shown in [8, 11], the defect-free state loses stability along the curve

$$\delta = \delta_1(\rho) = \frac{\pi^2}{\pi^2 + \log(\rho)^2}. \tag{15}$$

We next establish that the defect-free state undergoes a supercritical pitchfork bifurcation at $\delta = \delta_1$. Let $\delta = \delta_1 + \epsilon^2\tilde{\delta}$, where $0 < \epsilon \ll 1$, and consider perturbations of the form

$$\theta(r, \phi) = \theta^*(\phi) + \epsilon\eta_1(r, \phi) + \epsilon^3\eta_3(r, \phi) + \cdots, \tag{16}$$

where the functions $\eta_j(r, \phi)$ vanish on $r = \rho$, 1 and are 2π-periodic in ϕ. Substituting (16) into (4) and comparing terms of order ϵ, we find that

$$\mathcal{L}\eta_1 := (1 - \delta_1)\left(\eta_{1rr} + \frac{\eta_{1r}}{r}\right) + \frac{\eta_{1\phi\phi}}{r^2} + \frac{\delta_1\eta_1}{r^2} = 0. \tag{17}$$

From (14), we have that nontrivial solutions of (17) subject to homogeneous Dirichlet boundary conditions are given by

$$\eta_1 = A_1 \sin\left(\pi \frac{\log(r)}{\log(\rho)}\right), \tag{18}$$

where the amplitude A_1 is arbitrary.

Similarly, at order ϵ^3, we obtain the equation for η_3:

$$\begin{aligned}\mathcal{L}\eta_3 = {} & \frac{\left(\log(\rho)^2 + \pi^2\right) A_1 \left(\delta_1 A_1^2 - 2\tilde{\delta}\right)}{2r^2 \log(\rho)^2} \sin\left(\pi \frac{\log(r)}{\log(\rho)}\right) \\ & - \frac{\delta_1 A_1^3 \left(3\pi^2 + \log(\rho)^2\right)}{6r^2 \log(\rho)^2} \sin\left(3\pi \frac{\log(r)}{\log(\rho)}\right).\end{aligned} \tag{19}$$

The solvability condition for the inhomogeneous equation (19) subject to homogeneous Dirichlet boundary conditions is

$$A_1\left(A_1^2\delta_1 - 2\tilde{\delta}\right) = 0, \tag{20}$$

and thus the amplitude $A = \epsilon A_1$ is only defined for $\tilde{\delta} > 0$. Therefore, a supercritical pitchfork bifurcation occurs, with two nontrivial solution branches coming into existence as δ increases through $\delta_1(\rho)$.

The above weakly nonlinear analysis describes the bifurcation behavior when δ is close to δ_1 and the amplitude A is small. For larger values of A, we instead consider exact solutions of the Euler–Lagrange equations (4) for $\delta > \delta_1$. We seek an exact solution of the form

$$\theta(r, \phi; \delta) = \theta^*(\phi) + U(t; \delta), \qquad t = -\log r, \tag{21}$$

and find that U satisfies

$$2\left(1-\delta\cos^2 U\right)\ddot{U}+\delta\sin(2U)\left(\dot{U}^2+1\right)=0 \tag{22}$$

subject to $U(0;\delta)=U(-\log\rho;\delta)=0$, where the dot is used as shorthand for $\mathrm{d}/\mathrm{d}t$. We consider functions $U(t;\delta)$ with one stationary point, which must be at $t=(-\log\rho)/2$ by symmetry; solutions with more stationary points exist but have higher energy.

No generality is lost by assuming that $U>0$ for $t\in(0,-\log\rho)$ and thus that U achieves its maximum value, A say, at $t=(-\log\rho)/2$. Then (22) may be integrated twice to yield the implicit solution

$$\int_0^{U(t;\delta)}\sqrt{\frac{1-\delta\cos^2 u}{\delta\cos^2 u-\delta\cos^2 A}}\,\mathrm{d}u=t \tag{23}$$

for $0<t<(-\log\rho)/2$, where the amplitude A is related to ρ and δ by

$$\int_0^{A}\sqrt{\frac{1-\delta\cos^2 u}{\delta\cos^2 u-\delta\cos^2 A}}\,\mathrm{d}u=\frac{-\log\rho}{2}. \tag{24}$$

An analogous solution was obtained in [20] to describe the Fréedricksz transition in an annulus with strong perpendicular anchoring. For the special limiting case $\delta=1$, we can solve (22) exactly to find

$$U(1;t)=\cos^{-1}\left(\frac{\rho\mathrm{e}^{t}}{\rho+1}+\frac{\mathrm{e}^{-t}}{\rho+1}\right), \tag{25}$$

with associated amplitude

$$A=\cos^{-1}\left(\frac{2\sqrt{\rho}}{1+\rho}\right). \tag{26}$$

In Fig. 2(a), we plot the solution (21) for $\rho=0.2$ and $\delta=0.95$. We see that the director field appears spiral-like as it becomes energetically preferable for the director to splay instead of bend when δ is sufficiently large. The dependence of the solution amplitude A on the anisotropy δ and the radius ratio ρ is plotted in Fig. 2(b). For each fixed value of ρ, the base state $A=0$ is stable until $\delta=\delta_1(\rho)$, when the nontrivial solution branch appears via a supercritical pitchfork bifurcation. The amplitude then increases monotonically with δ, approaching the limiting value given by (26) as $\delta\to 1$.

The OF energy of the solution (21) is given by

$$E=2\pi\int_0^{A}(1+\delta\sin^2 A-2\delta\sin^2 u)\sqrt{\frac{1-\delta\cos^2 u}{\delta\cos^2 u-\delta\cos^2 A}}\,\mathrm{d}u, \tag{27}$$

while the energy of the defect-free state (9) is easily computed to be $E^{*}=\pi\log(1/\rho)$. Therefore, the transition from the defect-free state to the

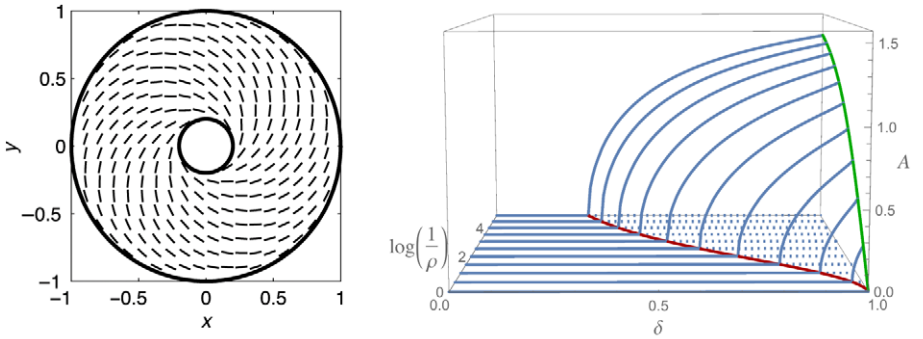

Figure 2. (a) The "spiral-like" director field for $\theta = \theta^* + U$, with $\rho = 0.2$ and $\delta = 0.95$. (b) The amplitude A versus δ and $\log(1/\rho)$. The red curve shows the bifurcation value $\delta = \delta_1(\rho)$; the green curve shows the amplitude (26) when $\delta = 1$.

spiral-like state results in an energy reduction

$$E^* - E = 2\pi\sqrt{\delta}\int_0^A (2\sin^2 u - \sin^2 A)\sqrt{\frac{1-\delta\cos^2 u}{\sin^2 A - \sin^2 u}}\,\mathrm{d}u. \tag{28}$$

It is an elementary exercise to prove that the integral on the right-hand side of (28) is positive for $\delta \in (0, 1)$ and $A \in (0, \pi/2)$. Therefore, the spiral-like state, when it exists, is energetically favorable compared to the defect-free state.

Moreover, we can verify that the spiral-like state is always a local minimizer of the OF energy (3) by analyzing the second variation

$$\begin{aligned}\delta^2 E &= \frac{\partial^2}{\partial\epsilon^2} E\left[\theta^* + U(t) + \epsilon\eta(t,\phi)\right]\Big|_{\epsilon=0} \\ &= \int_0^{2\pi}\int_0^{\log(1/\rho)} \Bigg\{(1-\delta)\left(\eta_t^2 + \eta_\phi^2\right) + \delta(\eta_t \sin U + \eta_\phi \cos U)^2 \\ &\quad - \left[\frac{(1+\dot{U}^2)\delta\big((2-\delta)\cos 2U - \delta\big)}{2(1-\delta\cos^2 U)}\right]\eta^2\Bigg\}\,\mathrm{d}t\,\mathrm{d}\phi.\end{aligned} \tag{29}$$

A classical minimizer $\eta_0(t)$ of (29) which is independent of ϕ satisfies the Euler–Lagrange equation

$$\frac{\mathrm{d}}{\mathrm{d}t}((1-\delta\cos^2 U)\dot{\eta}_0) + \left[\frac{(1+\dot{U}^2)\delta\big((2-\delta)\cos 2U - \delta\big)}{2(1-\delta\cos^2 U)}\right]\eta_0 = 0. \tag{30}$$

A solution of (30) which takes its maximum value at $t = (1/2)\log(1/\rho)$ is given by

$$\eta_0(t) = 1 - \dot{U}(t)\int_t^{(1/2)\log(1/\rho)} \frac{(1-\delta)\cos A\cos U(t') - \sin A\sin U(t')}{\sin(A+U(t'))(1-\delta\cos^2 U(t'))}\,\mathrm{d}t', \tag{31}$$

and it is easily shown that $\eta_0(t)$ so defined is positive for $t \in (0, \log(1/\rho))$. Therefore, we can make the substitution $\eta(t,\phi) = \eta_0(t)\zeta(t,\phi)$ in (29) to find

$$\delta^2 E = \int_0^{2\pi}\int_0^{\log(1/\rho)} \left\{(1-\delta)\left(\zeta_t^2 + \zeta_\phi^2\right) + \delta(\zeta_t \sin U + \zeta_\phi \cos U)^2\right\}\eta_0^2\,\mathrm{d}t\,\mathrm{d}\phi, \tag{32}$$

and we deduce that $\delta^2 E > 0$ for nontrivial perturbations.

To summarize, the defect-free state loses stability to the energetically preferable spiral-like state when $\delta > \delta_1(\rho)$. However, with strong anchoring, there is no possibility of secondary bifurcation to an equilibrium state that depends on the polar angle ϕ, as in the experimentally observed director fields illustrated in Fig. 1. Therefore, in the next section we investigate the effects of relaxing the strong anchoring boundary conditions.

3.3. Weak anchoring

In this section, we consider the effects of weak anchoring and study the stability of the defect-free state in (9) in terms of anchoring strength, elastic anisotropy, and annular aspect ratio. The purely radially symmetric linear stability analysis may be found in [12]. We extend the analysis to nonradially symmetric perturbations and also compute new stability diagrams that quantify the sensitivity of the defect-free state to different types of perturbations.

One can easily check that the OF defect-free state θ^*, in Eq. (9), is a solution of (4) with the weak boundary conditions (7)–(8). By analogy with Section 3.2, we compute the second variation of the OF energy in (3) and the surface energy in (6) to be

$$\delta^2 E[\theta^*] := \int_\Omega (\nabla\eta)^2 - \delta\left(\frac{\eta}{r} + \eta_r\right)^2 \mathrm{d}\Omega + \alpha\int_{\partial\Omega}\eta^2\,\mathrm{d}\sigma, \tag{33}$$

where η is a perturbation about θ^*. It is clear from (33) that $\delta > 0$ is a necessary condition for $\delta^2 E$ to be negative and thus for the defect-free state to lose stability. Without loss of generality, we can expand the perturbation in the form $\eta(r,\phi) = \sum_k f_k(t)\mathrm{e}^{\mathrm{i}k\phi}$, where $t = -\log r$ and $k = 0, 1, \cdots$ is referred to as the azimuthal order of the perturbation. For each k, the

optimal f_k is a solution of

$$\ddot{f}_k(t) + \frac{\delta - k^2}{1-\delta} f_k(t) = 0, \tag{34}$$

with boundary conditions

$$\dot{f}_k(t) = \frac{\alpha - \delta}{1-\delta} f_k(t) \text{ on } t = 0, \quad \dot{f}_k(t) = -\frac{\alpha\rho + \delta}{1-\delta} f_k(t) \text{ on } t = \log(1/\rho). \tag{35}$$

The general solution of (34) is

$$f_0(t) = A \sin\left(\sqrt{\frac{\delta}{1-\delta}}\, t\right) + B \cos\left(\sqrt{\frac{\delta}{1-\delta}}\, t\right) \quad \text{for } k = 0, \tag{36}$$

$$f_k(t) = A \sinh\left(\sqrt{\frac{k^2-\delta}{1-\delta}}\, t\right) + B \cosh\left(\sqrt{\frac{k^2-\delta}{1-\delta}}\, t\right) \quad \text{for } k \geq 1, \tag{37}$$

and the boundary conditions (35) lead to the following compatibility condition between α, δ, ρ, and the order k of the perturbation:

$$\tan\left(\sqrt{\frac{\delta}{1-\delta}} \log\left(\frac{1}{\rho}\right)\right) + \frac{\alpha(1+\rho)\sqrt{\delta(1-\delta)}}{\alpha\delta - \alpha\rho\delta + \alpha^2\rho - \delta} = 0 \quad \text{for } k = 0, \tag{38}$$

$$\tanh\left(\sqrt{\frac{k^2-\delta}{1-\delta}} \log\left(\frac{1}{\rho}\right)\right) + \frac{\alpha(1+\rho)\sqrt{(k^2-\delta)(1-\delta)}}{\delta\alpha + \alpha^2\rho - \alpha\rho\delta - \delta + k^2(1-\delta)} = 0$$

$$\text{for } k \geq 1. \tag{39}$$

For a given $k \in \mathbb{N}$, there are typically multiple solutions $\{\delta_{1,k}, \delta_{2,k}, \ldots\}$ of the compatibility relations (38) and (39). We are interested in the smallest solution, $\delta_{1,k}$, such that the defect-free state loses stability for $\delta > \delta_{1,k}(\rho)$ for a fixed k.

The case $k = 0$ has been dealt with in [12]. The compatibility condition (38) has an infinite number of solutions $\{\delta_{1,0}, \delta_{2,0}, \cdots, \}$ for any fixed triplet $\{\alpha > 0,\ \delta \in (0,1),\ \rho \in (0,1)\}$, and the corresponding eigenfunctions are

$$f_{n,0}(t) = \sin\left(\sqrt{\frac{\delta_{n,0}}{1-\delta_{n,0}}}\, t\right) + \frac{\sqrt{\delta_{n,0}(1-\delta_{n,0})}}{\alpha - \delta_{n,0}} \cos\left(\sqrt{\frac{\delta_{n,0}}{1-\delta_{n,0}}}\, t\right). \tag{40}$$

In Fig. 3, we plot the smallest eigenvalue $\delta_{1,0}$ as a function of ρ, for different values of α. As $\alpha \to \infty$, the strong anchoring limit (14) is recovered, and $\delta_{1,0} \to \delta_1(\rho)$ given by (15). By following the weakly

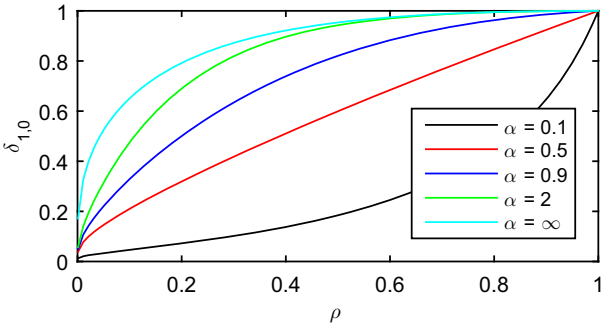

Figure 3. The first eigenvalue $\delta_{1,0}$ plotted versus ρ for various fixed values of α. The strong anchoring result (15) is recovered in the limit $\alpha \to \infty$.

nonlinear analysis from Section 3.2, we can show that the loss of stability again occurs through a supercritical pitchfork bifurcation at $\delta = \delta_{1,0}$.

For $k = 1$, the compatibility condition (39) has a unique solution

$$\delta_{1,1}(\alpha, \rho) = \frac{\alpha\rho^2 + \alpha^2\rho + \alpha + 1 - \rho^2\alpha^2 - \rho}{2(\alpha\rho - \rho + 1)}. \tag{41}$$

It is straightforward to show that $\delta_{1,1} \in (0, 1)$ if and only if $0 < \alpha < 1$, and that $\delta_{1,1} > 1/2$ for all ρ. For $k > 1$, the compatibility condition (39) has solutions for $\delta \in (0, 1)$ only if $\alpha < 1$. Therefore, the defect-free state can be unstable to ϕ-dependent azimuthal perturbations with $k \geq 1$ only if the anchoring strength is small enough that $\alpha < 1$. The critical value $\alpha = 1$ corresponds to a very small chamber with $R_{\text{outer}} = \xi$, so the chamber radius is equal to the surface extrapolation length. For macroscopic domains with $R_{\text{outer}} > \xi$, the defect-free state can only be destabilized by radial perturbations and azimuthal variations may be neglected.

In Fig. 4, we plot the stability curves described by the eigenvalues, $\delta = \delta_{1,k}$, in the (δ, α)-plane, for fixed values of k and ρ. It is evident from the plots that, as δ increases, the defect-free state first loses stability with respect to the $k = 0$ mode. If the anchoring strength is small enough that $\alpha < 1$, then subsequent bifurcations lead to the possibility of ϕ-dependent perturbations. However, to get higher values of k, we need α to be smaller than 1 and δ to be sufficiently close to unity, namely, $\delta_{1,k} > k^2/(k^2 + 1)$, which is the limit of $\delta_{1,k}$ as $\alpha \to 0$. In contrast, the experiments reported in [4] exhibit stable nonaxisymmetric equilibria with boundary defects for δ close to zero (almost isotropic materials), with moderate values of α and ρ. Furthermore, these states may be bistable with the defect-free state. Hence, we deduce that the experimentally observed equilibria with boundary defects are not a natural consequence of the loss of stability of the defect-free state, and we study them independently in Section 4.

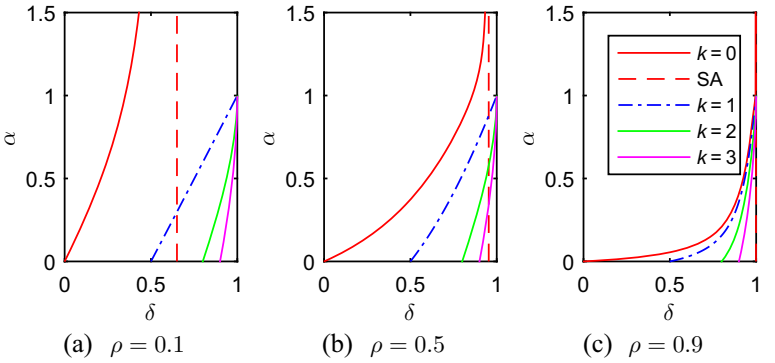

(a) $\rho = 0.1$ (b) $\rho = 0.5$ (c) $\rho = 0.9$

Figure 4. The smallest solution $\delta_{1,0}$ to the $k = 0$ compatibility condition (38), and the only solution to (39) for $k = 1, 2, 3$ in the (δ, α)-plane for fixed ρ. The strong anchoring (SA) limit $\delta = \delta_1(\rho)$ is shown using dashed lines.

4. Nematic equilibria with boundary defects

4.1. Problem setup

In this section, we model states with tangential boundary conditions and regularly spaced defects located on the boundary, such as those shown in Figs. 1(b) and (c). To model such states, we partition Ω into $N \in \mathbb{N}$ sectors, and define the sector Ω_N to be

$$\Omega_N := \left\{ (r, \phi) \in \mathbb{R}^2 : \rho \leq r \leq 1,\ 0 \leq \phi \leq \frac{2\pi}{N} \right\}. \tag{42}$$

We work with tangential anchoring on the boundary of Ω, which in the strong anchoring limit corresponds to Dirichlet conditions of the form (5) on the curved edges of Ω_N ($r = \rho$ and $r = 1$). On the two straight edges of Ω_N ($\phi = 0$ and $\phi = 2\pi/N$), we assume that the director field is constant and tangent to these edges. These conditions correspond to $\theta = 0$ on $\phi = 0$ and $\theta = 2\pi/N + n\pi$ on the edge $\phi = 2\pi/N$, where $n \in \mathbb{Z}$. These boundary conditions necessarily induce discontinuities at the four corners of Ω_N. In the strong anchoring case, we only consider states with minimal corner defects, i.e., the director rotates by the minimal amount between the two edges and the corner defects are either of the "splay" type or the "bend" type. The director profile splays outward near a splay vertex and the director profile bends around a vertex for a bend vertex. We note that the assumed symmetry of the overall configuration in Ω could also be enforced by imposing normal boundary conditions on the straight edges of Ω_N, but the resulting state would not exhibit the boundary defects observed in experimental results and shown schematically in Fig. 1.

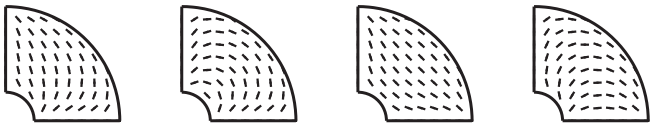

The D state. The U_1 state. The U_2 state. The U_3 state.

Figure 5. The director field of the four states within Ω_4 with $\rho = 0.25$ in the one-constant approximation.

There are four distinct arrangements of defects at the corners, $\partial\Omega_N$, as shown in Fig. 5. Three of these arrangements are generalizations of the rotated state in square and rectangular wells [15, 16, 21], denoted by U_1, U_2, and U_3, respectively, where the director field connects two adjacent splay defects along an edge, and the fourth arrangement is a generalized diagonal state, D, for which the director field connects two diagonally opposite splay defects. The two splay defects lie at the vertices of the $r = \rho$ edge for the U_1 state, at the vertices of the $r = 1$ edge for U_2, and at the vertices of the $\phi = 0$ edge, for U_3. Other rotated and diagonal states are equivalent under rotations or reflections to one of the four cases enumerated in Fig. 5.

We only consider these four possibilities, assume that each sector has the same configuration and define an overall configuration in Ω as the superposition of the different sector configurations on Ω_N, glued along their common edges. For a given N, we can typically generate multiple states using this principle of gluing together sector configurations, but for odd N, a superposition of D or U_3 states does not work as it requires the presence of a splay and bend-type defect simultaneously at one of the vertices.

4.2. The one-constant approximation with strong anchoring

We start with the one-constant approximation, for which $\delta = 0$, and the OF energy (3) reduces to

$$E[\theta] := \frac{1}{2}\int_{\Omega} |\nabla\theta|^2 \, \mathrm{d}\Omega. \tag{43}$$

We define the sector configurations to be solutions of the Laplace equation, $\nabla^2\theta = 0$ on Ω_N. Any admissible θ, subject to the Dirichlet boundary conditions discussed in Section 4.1, can be written as

$$\theta = a_0\phi + a_1 f_1 + a_2 f_2 + a_3 f_3 + a_4 f_4, \tag{44}$$

where the canonical functions f_i are solutions of the Laplace equation with boundary conditions:

- $f_1(r, 0) = f_1(r, 2\pi/N) = f_1(\rho, \phi) = 0$ and $f_1(1, \phi) = 1$;
- $f_2(r, 0) = f_2(r, 2\pi/N) = f_2(\rho, \phi) = 0$ and $f_2(1, \phi) = \phi$;

Table 1
Values of the Coefficients a_i for the Four Sector Solutions within Ω_N

State	a_0	a_1	a_2	a_3	a_4
D	1	$\frac{\pi}{2}$	0	$\frac{\pi}{2}$	0
U_1	$1+\frac{N}{2}$	$\frac{\pi}{2}$	$-\frac{N}{2}$	$\frac{\pi}{2}$	$-\frac{N}{2}$
U_2	$1-\frac{N}{2}$	$-\frac{\pi}{2}$	$\frac{N}{2}$	$-\frac{\pi}{2}$	$\frac{N}{2}$
U_3	1	$-\frac{\pi}{2}$	0	$\frac{\pi}{2}$	0

- $f_3(r,0) = f_3(r,2\pi/N) = f_3(1,\phi) = 0$ and $f_3(\rho,\phi) = 1$;
- $f_4(r,0) = f_4(r,2\pi/N) = f_4(1,\phi) = 0$ and $f_4(\rho,\phi) = \phi$.

The corresponding values of $a_0, a_1, \cdots, a_4$ for the four sector configurations are listed in Table 1.

The canonical functions, $f_1, \ldots, f_4$, can be computed using separation of variables as shown below:

$$f_1(r,\phi) = \sum_{n=1}^{\infty} \frac{4\sin\big((n-1/2)N\phi\big)}{(2n-1)\pi} \times \times \left[\frac{r^{-(n-1/2)N} - \rho^{-(2n-1)N} r^{(n-1/2)N}}{1-\rho^{-(2n-1)N}}\right], \tag{45}$$

$$f_2(r,\phi) = \sum_{n=1}^{\infty} \frac{4(-1)^{n+1}\sin\big(Nn\phi/2\big)}{Nn} \left[\frac{r^{-nN/2} - \rho^{-nN} r^{nN/2}}{1-\rho^{-nN}}\right], \tag{46}$$

$$f_3(r,\phi) = \sum_{n=1}^{\infty} \frac{4\sin\big((n-1/2)N\phi\big)}{(2n-1)\pi} \left[\frac{r^{-(n-1/2)N} - r^{(n-1/2)N}}{\rho^{-(2n-1)N/2} - \rho^{(2n-1)N/2}}\right], \tag{47}$$

$$f_4(r,\phi) = \sum_{n=1}^{\infty} \frac{4(-1)^{n+1}\sin\big(Nn\phi/2\big)}{Nn} \left[\frac{r^{-nN/2} - r^{nN/2}}{\rho^{-nN/2} - \rho^{nN/2}}\right]. \tag{48}$$

Some sample director plots calculated using these canonical functions are shown in Fig. 5 for $N = 4$ and $\rho = 0.25$.

Due to the discontinuities in θ at the corners of Ω_N, we regularize the domain by removing quarter-disks of radius ϵ about each of the vertices

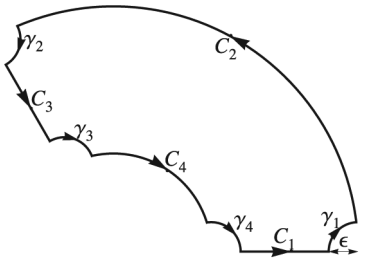

Figure 6. Schematic of the regularized domain $\Omega_{N\epsilon}$. The edges of the original sector region Ω_N are denoted $C_1, \cdots, C_4$. The vertices of Ω_N are replaced by four small circular arcs $\gamma_1, \cdots, \gamma_4$ of radius $\epsilon \ll \rho$.

(to prevent the energy (43) from diverging) and denote the new regularized domain by $\Omega_{N\epsilon}$, as illustrated in Fig. 6. The length ϵ is proportional to the defect core size [22], and we assume that $\epsilon \ll \rho$. An analogous approach was used in [16] to evaluate the regularized OF energy in a rectangular domain. The boundary, $\partial\Omega_{N\epsilon}$, consists of four edges, $C_1, \ldots, C_4$, and four curved arcs of radius ϵ (enclosing the corners) denoted by $\gamma_1, \ldots, \gamma_4$, respectively. We use Green's First Identity to obtain

$$E = \frac{1}{2}\oint_{\partial\Omega_{N_\epsilon}} \theta\nabla\theta \cdot \mathbf{v}\,\mathrm{d}\sigma = \sum_{i=1}^{4}\left[\frac{1}{2}\int_{C_i} \theta\nabla\theta \cdot \mathbf{v}\,\mathrm{d}\sigma + \frac{1}{2}\int_{\gamma_i} \theta\nabla\theta \cdot \mathbf{v}\,\mathrm{d}\sigma\right], \quad (49)$$

where $\mathbf{v}$ is the outward pointing normal to each boundary segment.

Although $\nabla\theta$ diverges at each vertex, $\nabla\theta \cdot \mathbf{v}$ is zero to lowest order on each arc γ_i, and it can be shown that the energetic contributions from γ_i in (49) are of order ϵ as $\epsilon \to 0$. We define four functions related to the energy contributions from the edges C_i, namely,

$$s_1(N, \rho) := \sum_{n=1}^{\infty} \frac{\coth\big(N(n-1/2)\log\rho\big) + 1}{n - \frac{1}{2}}, \quad (50)$$

$$s_2(N, \rho) := \sum_{n=1}^{\infty} \frac{\coth\big((Nn/2)\log\rho\big) + 1}{n/2}, \quad (51)$$

$$s_3(N, \rho) := \sum_{n=1}^{\infty} \frac{\operatorname{cosech}\big(N(n-1/2)\log\rho\big)}{n - \frac{1}{2}}, \quad (52)$$

$$s_4(N, \rho) := \sum_{n=1}^{\infty} \frac{\operatorname{cosech}\big((Nn/2)\log\rho\big)}{n/2}. \quad (53)$$

As $\epsilon \to 0$, the regularized energy within $\Omega_{N\epsilon}$ is then given by

$$E \sim \pi \log\left(\frac{1}{\epsilon}\right) + \pi \tilde{E} + O(\epsilon), \tag{54}$$

where the normalized energy, $\tilde{E}$, is the interior distortion energy and the logarithmic term is the "defect energy" and is identical for all four states. The normalized energies of the four states are given by

$$\begin{aligned}\tilde{E}_{U_1} &= s_1(N,\rho) + s_4(N,\rho) - s_2(N,\rho) - s_3(N,\rho) \\ &\quad + \frac{(N+2)^2}{4N}\log\left(\frac{1}{\rho}\right) + \frac{1}{2}\log\left(\frac{\rho}{N^2}\right),\end{aligned} \tag{55}$$

$$\begin{aligned}\tilde{E}_{U_2} &= s_1(N,\rho) + s_4(N,\rho) - s_2(N,\rho) - s_3(N,\rho) \\ &\quad + \frac{(N-2)^2}{4N}\log\left(\frac{1}{\rho}\right) + \frac{1}{2}\log\left(\frac{\rho}{N^2}\right),\end{aligned} \tag{56}$$

$$\tilde{E}_{U_3} = -s_1(N,\rho) - s_3(N,\rho) + \frac{1}{N}\log\left(\frac{1}{\rho}\right) + \frac{1}{2}\log\left(\frac{16\rho}{N^2}\right), \tag{57}$$

$$\tilde{E}_D = s_3(N,\rho) - s_1(N,\rho) + \frac{1}{N}\log\left(\frac{1}{\rho}\right) + \frac{1}{2}\log\left(\frac{16\rho}{N^2}\right). \tag{58}$$

In Fig. 7, we plot the normalized energy of each of the four sector configurations, as a function of N, for some fixed values of ρ. For small values of N, the U_2 state is the minimum energy state in this set $\{U_1, U_2, U_3, D\}$. In contrast, for a square or rectangle, the diagonal state always has the minimum normalized energy [16]. As N increases, there is an energy cross-over and the D state has the minimum normalized energy for large N, since Ω_N approaches a rectangle as $N \to \infty$.

Using the expressions (55)–(58) for the normalized energies, we can numerically evaluate the cross-over critical value $N = N_c(\rho)$, at which $\tilde{E}_{U_2} = \tilde{E}_D$. As shown in Fig. 8, N_c is a monotonic increasing function of ρ, tending to infinity as $\rho \to 1$. For moderate values of $\rho \geq 0.4$, the rotated state U_2 minimizes the energy in the sector Ω_N for $N \leq 10$. As $\rho \to 0$, the series $s_1, \cdots, s_4$ become negligible, and thus N_c may be estimated as

$$N_c(\rho) \sim 4 + \frac{8\log 2}{\log(1/\rho)} \quad \text{as } \rho \to 0, \tag{59}$$

which is plotted in Fig. 8 as a dashed curve. Thus, U_2 is the energetically preferred state for $N \leq 4$ regardless of the size of ρ.

We define a sector-based OF equilibrium to be a superposition of the sector configurations on Ω_N, glued along the common edges of Ω_N. We

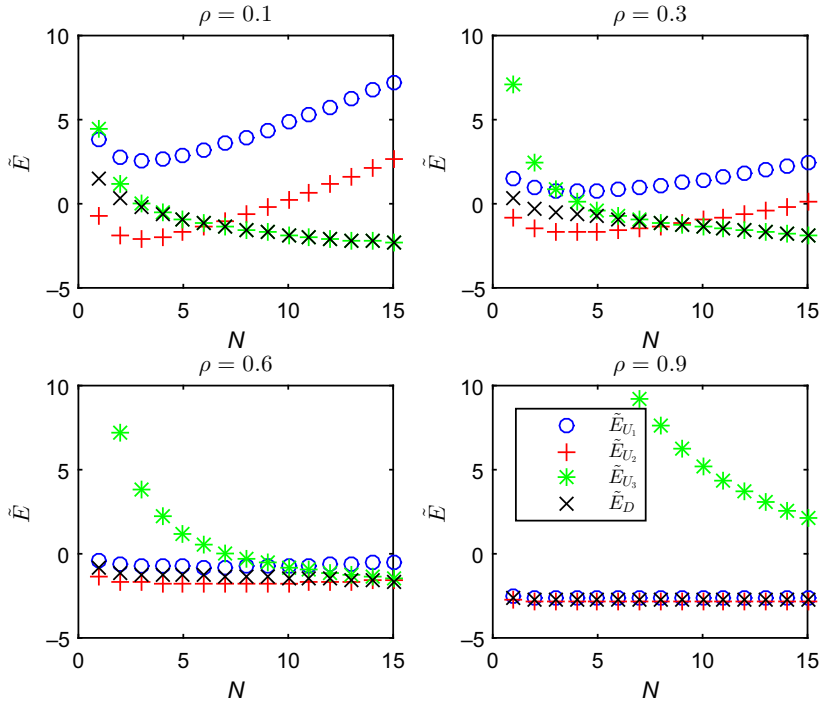

Figure 7. The normalized energies of the four states $\{U_1, U_2, U_3, D\}$ in Ω_N, plotted against N, for fixed values of ρ.

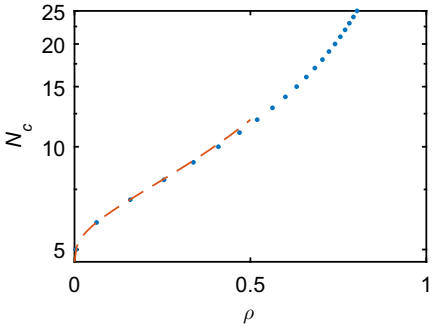

Figure 8. The critical cross-over value of $N = N_c(\rho)$ versus aspect ratio ρ. The dashed curve shows the asymptotic estimate (59).

compare the energies of the sector-based equilibria on the annulus Ω, which is simply the OF energy of a sector configuration multiplied by N-the number of sectors, since we have assumed that all sectors are identical. Figure 9 displays the energies of the two lowest energy sector-based equilibria with defects, namely, the U_2 states with $N = 1$ and $N = 2$, plotted

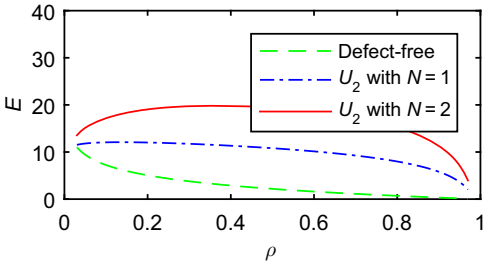

Figure 9. The one constant Oseen–Frank energy of the defect-free state and the U_2 states with $N = 1, 2$ versus aspect ratio ρ, for defect core size $\epsilon = 0.01$.

versus ρ with $\epsilon = 0.01$. Also shown as a dashed curve is the energy of the defect-free state. We observe that the defect-free state always has lesser energy than the competing sector-based equilibria, except in the regime where $\rho = O(\epsilon)$.

In the limit where $\rho = O(\epsilon)$ and $\epsilon \to 0$, the defect-free state has a vortex at the origin, the U_2 state with $N = 1$ approaches a state with a $+1/2$ defect at the origin and a $+1/2$ defect on the outer boundary and the U_2 state with $N = 2$ tends to a state with two $+1/2$ defects pinned to the outer boundary. In this limit, the asymptotic approximations (55)–(58) cease to be valid, but one can check that the defect-free state with an approximate vortex at the origin has higher energy than the U_2 state (with $N = 2$ and $N = 1$, respectively) if ρ/ϵ is sufficiently small. We argue that such microscopic values of ρ are not experimentally relevant, and these observations do not suffice to explain the experimental stability of states with boundary defects. In the following subsections, we introduce further physical effects, namely, elastic anisotropy and weak anchoring, which allow configurations with defects to be energetically preferable to the defect-free state for realistic values of ρ.

4.3. Elastic anisotropy with strong anchoring

We use the commercially available software COMSOL Multiphysics to numerically solve the Euler–Lagrange equation (4) with $\delta \neq 0$, and strong tangential anchoring conditions on $\partial\Omega_N$. We find analogs of all four states $\{U_1, U_2, U_3, D\}$, with qualitatively similar structures to the $\delta = 0$ case. As in Section 4.2, we define the anisotropic versions of the sector configurations and sector-based equilibria and numerically compute the corresponding OF energies, using an effective core radius $\epsilon \ll 1$. We evaluate the regularized energy in Ω_N, compute the total energy in Ω as before and compare with the energy of the defect-free state. In Fig. 10, we compare the energies of the defect-free state, the spiral-like state discussed in Section 3.2 and

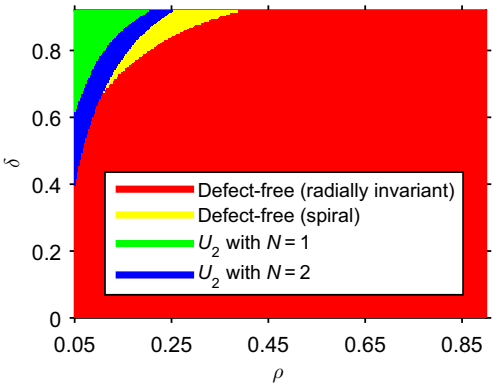

Figure 10. The (ρ, δ) parameter space with $\epsilon = 0.01$. We compare the energies of the U_2 states with $N = 1$, 2; the defect-free state; and the spiral-like state and the shaded regions label the state with the minimal energy, restricted to these four competing configurations, on Ω.

the U_2 sector-based equilibrium with $N = 2$ and $N = 1$ (with $\delta \neq 0$) and show for $\epsilon = 0.01$, the regions of the (ρ, δ) parameter space where each of the four candidate states is energetically preferred (compared to the other competing states). This is not an exhaustive study since we only focus on four representative states. The region of the parameter space for which the U_2 states are energetically preferable is dependent on ϵ, decreasing ϵ will make this section of the parameter space smaller.

For δ sufficiently close to 1, the defect-free state need not be the global minimizer of the OF energy. As the value of ρ decreases, the defect-free state first loses stability to the spiral-like state, as shown in Section 3.2. For yet smaller values of ρ, the states with defects become energetically preferable, first with $N = 2$ and then with $N = 1$. This energy cross-over demonstrates that elastic anisotropy may stabilize states with boundary defects for experimentally realistic values of ρ.

4.4. The one-constant approximation with weak anchoring

The experiments reported in [4, 5] do not use highly anisotropic materials. A second mechanism for stabilization of boundary defects is weak anchoring. We consider the annular sector Ω_N, with weak anchoring on the edges at $r = \rho$, 1 and strong tangential anchoring on the edges at $\phi = 0$, $2\pi/N$. The corresponding "weak" analog of the U_2-sector configuration are solutions of $\nabla^2\theta = 0$ subject to the boundary conditions

$$\frac{\partial\theta}{\partial r} = \frac{\alpha}{2}\sin(2\theta - 2\phi) \text{ at } r = 1, \ \theta = 0 \text{ at } \phi = 0, \tag{60}$$

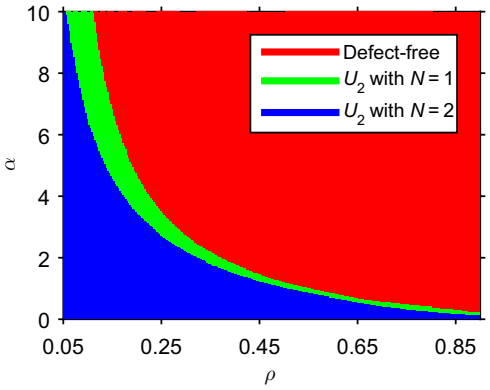

Figure 11. The (ρ, α) parameter space. We compare the energies of the U_2 states with $N = 1$, 2 and the defect-free state and the shaded regions label the minimal energy state, restricted to these three competing configurations, on Ω.

$$\frac{\partial \theta}{\partial r} = -\frac{\alpha}{2} \sin(2\theta - 2\phi) \text{ at } r = \rho, \ \theta = \frac{2\pi}{N} - \pi \text{ at } \phi = \frac{2\pi}{N}. \tag{61}$$

We use COMSOL to solve the Laplace equation in Ω_N with boundary conditions (60)–(61) and evaluate the corresponding energy for given values of α and ρ. Weak anchoring serves to regularize the boundary defects so that the OF energy is finite, and there is no longer any need to introduce the defect core size ϵ.

In Fig. 11, we compare the energies of the defect-free state, and the weak analog of the U_2 sector-based equilibrium with either $N = 1$ or $N = 2$. We plot a phase diagram which demarcates the parameter regimes (ρ, α), (with $\delta = 0$) for which states with boundary defects are energetically preferred to the defect-free state. When the dimensionless anchoring strength α is large, the defect-free state is preferred unless ρ is extremely small, as expected from the strong anchoring results in Section 3.2. However, as the surface anchoring becomes weaker, states with boundary defects become energetically preferable, even at relatively large values of the ratio ρ. This suggests that, particularly in systems with low elastic anisotropy, i.e., small δ, the role of weak anchoring at the cell boundaries should be considered when interpreting experimental observations of equilibria with boundary defects.

4.5. States with boundary defects in LdG theory

In the preceding subsections, we construct sector-based equilibria on an annulus, Ω, by gluing together sector configurations on Ω_N along their

common edges. It is natural to ask if we can have real nematic equilibria, or even transient states, in a dynamic evolution that retain the symmetries of our sector-based equilibria. If such states persist over a length of time, they are of experimental relevance and may explain the experimental observations of states with boundary defects in annular chambers.

The question of interest then is—can we have OF equilibria on Ω that retain the symmetries of the sector configurations? To address this question, we work in a 2D LdG framework that incorporates a director field, **n** and a scalar order parameter s, analogous to the framework used in [23, 24]. The scalar order parameter regularizes the defects, so that the LdG acts as a weighted OF model. We describe the nematic state by a symmetric, traceless 2×2 matrix: the reduced LdG **Q**-tensor is given by

$$\mathbf{Q} = \begin{pmatrix} q_1 & q_2 \\ q_2 & -q_1 \end{pmatrix}. \tag{62}$$

We note that there is no biaxiality in this simple model since we do not aim to resolve defect structures but rather focus on structural symmetries away from defects.

To simulate weak anchoring, we incorporate a Durand–Nobili surface energy into the normalized LdG energy [23, 25] to obtain the rescaled energy functional

$$\begin{aligned} E[q_1, q_2] \;=\; & \int_\Omega |\nabla q_1|^2 + |\nabla q_2|^2 + \frac{1}{4\epsilon^2}\left(2q_1^2 + 2q_2^2 - 1\right)^2 \,\mathrm{d}\Omega \\ & + \alpha \int_{\partial\Omega} \left(q_1 + \frac{\cos(2\phi)}{\sqrt{2}}\right)^2 + \left(q_2 + \frac{\sin(2\phi)}{\sqrt{2}}\right)^2 \,\mathrm{d}\sigma, \end{aligned} \tag{63}$$

where α is again the dimensionless anchoring strength and $\varepsilon^2 = L/|A|$ (L is the elastic constant and A is proportional to the temperature.) We adopt the gradient-flow model for $E[q_1, q_2]$ to investigate the evolution of states subject to initial conditions with the sector symmetries discussed in Section 4.2. We therefore solve the system

$$-\frac{\partial q_i}{\partial t} + \nabla^2 q_i = \frac{q_i}{\varepsilon^2}\left(2q_1^2 + 2q_2^2 - 1\right) \tag{64}$$

in Ω subject to boundary conditions

$$\frac{\partial q_1}{\partial \mathbf{v}} + \alpha\left(q_1 + \frac{\cos(2\phi)}{\sqrt{2}}\right) = 0, \qquad \frac{\partial q_2}{\partial \mathbf{v}} + \alpha\left(q_2 + \frac{\sin(2\phi)}{\sqrt{2}}\right) = 0 \tag{65}$$

on $\partial\Omega$.

We now use the sector configurations to construct initial conditions for the **Q**-tensor, namely,

$$q_1 = s\cos(2\theta), \qquad q_2 = s\sin(2\theta) \tag{66}$$

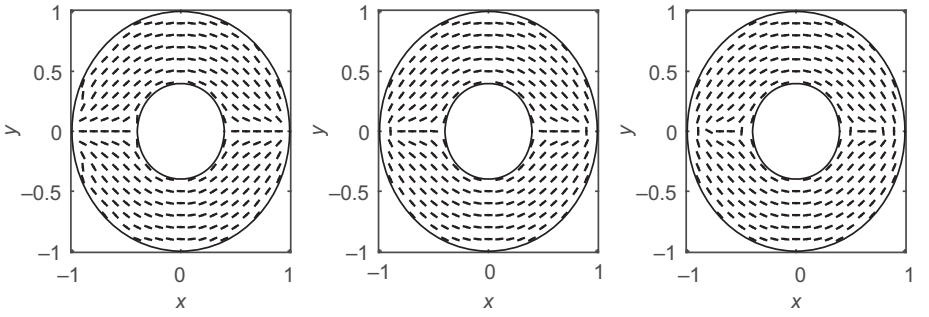

(a) Initial condition. (b) $t = 0.04$ (c) $t = 0.08$

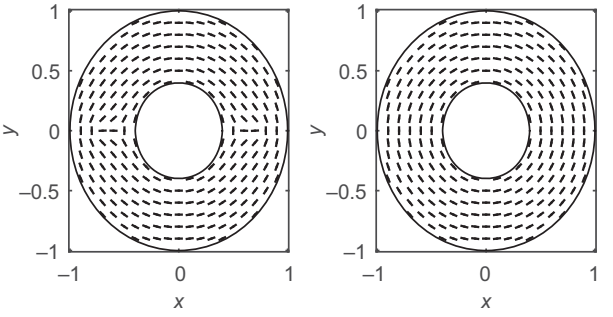

(d) $t = 0.12$ (e) $t = 0.16$

Figure 12. Initial condition ($t = 0$) and snapshots of the director at variable t, with $\epsilon = 0.01$, $\rho = 0.4$, and $\alpha = 50$.

at $t = 0$, where θ is a sector-based equilibrium as discussed in Section 4.2 obtained by gluing together OF sector solutions of the form (44). The initial order parameter s is defined to be $1/\sqrt{2}$ everywhere except in a disk of radius 3ϵ about each initial defect location $\mathbf{r}_k$, where we set $s = |\mathbf{r} - \mathbf{r}_k|/(3\epsilon\sqrt{2})$.

We use COMSOL to solve (64) subject to (65) and the above initial conditions, and investigate the long-time dynamics of the system as $t \to \infty$. For suitably large values of α, the initial defects detach from the edges, approach and annihilate each other, so the system ultimately approaches the defect-free state, for example, see Fig. 12. Here, the order parameter (not shown) is approximately equal to $1/\sqrt{2}$ everywhere except in a small radius about the defects.

However, for small values of α, the defects do not always detach from the boundary. Some example solutions are shown in Fig. 13 with $\rho = 0.4$, $\epsilon = 0.01$, and $N = 2$. Panel (a) shows a converged solution with $\alpha = 10$. At this relatively low value of the anchoring strength, the initial boundary defects move outside the domain, resulting in much weaker

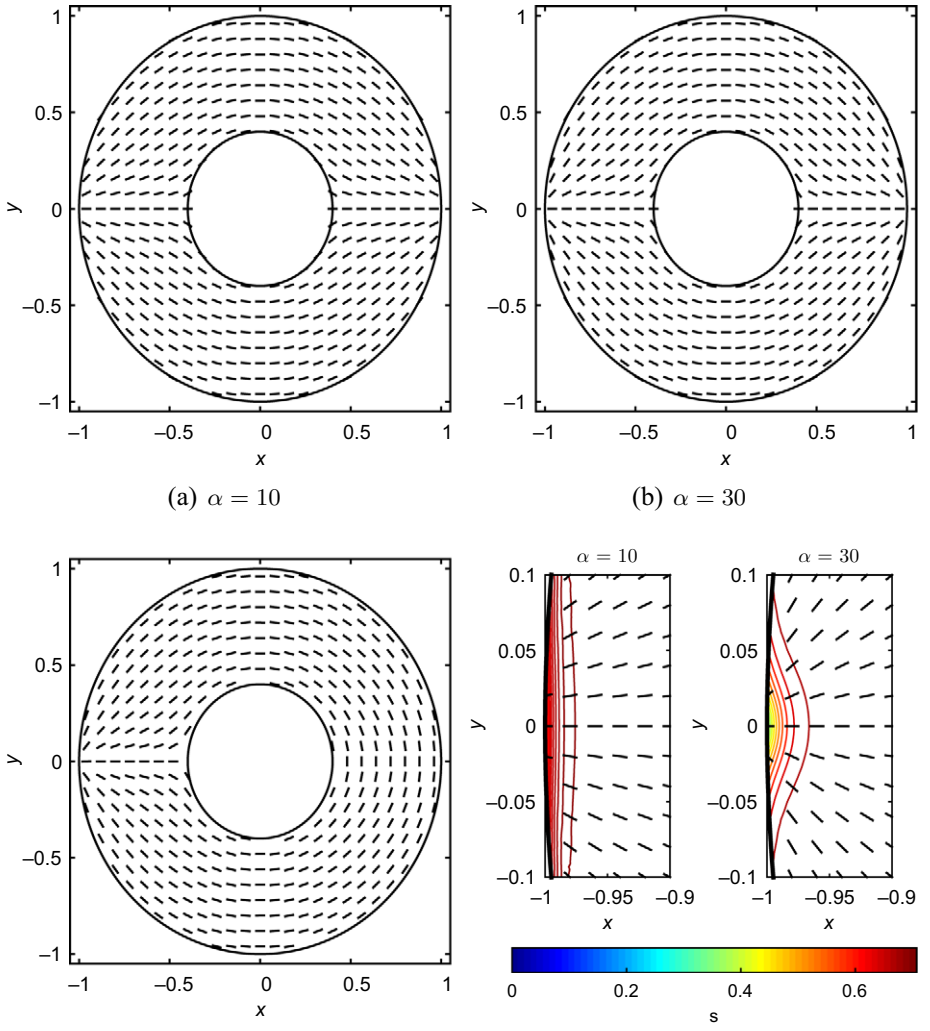

(a) $\alpha = 10$ (b) $\alpha = 30$

(c) $\alpha = 40$ (d) Close-up of $(-1, 0)$ for $\alpha = 10$, 30.

Figure 13. Converged solutions of Eqn. (64) with $\rho = 0.4, \epsilon = 0.01$, and variable α, subject to boundary conditions (65) with initial conditions given by the U_2 state with $N = 2$. The local behaviors of the director (dashed lines) and order parameter (colored contours) about the defects at $(-1, 0)$ from (a) and (b) are shown in (d).

energy concentrations at the initial defect points and an order parameter approximately equal to $1/\sqrt{2}$ even at the boundary (see (d)). In panel (b), the anchoring strength α is increased to 30, resulting in somewhat stronger approximate defects on the boundaries. The fine structure of the director and order parameter about one of the defects is shown in (d). In both cases (a) and (b), the overall structure of the initial state, with symmetry lines

at $\phi = 0, \pi$, is preserved by the dynamics. In panel (c), with anchoring strength $\alpha = 40$, we find that a single pair of defects detach and annihilate in a similar process to that shown in Fig. 12, leaving a state that resembles the U_2 state with $N = 1$. The remaining pair of defects remain anchored to the wall, with a similar order parameter profile to that of $\alpha = 30$.

These numerical results illustrate how, for moderate values of ρ and moderate values of α, initial conditions constructed from the sector configurations in Section 4.2 generate dynamic solutions which retain approximate singularities, reminiscent of $\pm 1/2$ defects, at the sector vertices for long times. For these combinations of coefficients, these solutions with boundary defects (or virtual defects near boundaries) and rotational symmetries are not the global minimizer as the defect-free state always has a lower energy; therefore the solutions are at most metastable. We do not make any conclusions about the exact defect profiles and if they are pinned to the boundaries. These numerical investigations simply suggest that there do exist (approximate) OF equilibria that have the sector symmetries discussed in Section 4.2 and, hence, our sector-based equilibria are a useful construction for studying experimental states with boundary defects which share the sectorial symmetries of the analytic constructions in Section 4.2.

5. Conclusions

In this paper, we study nematic equilibria on a 2D annulus, with strong or weak tangential anchoring, modeled in the continuum OF theoretical framework. We use formal perturbation methods to obtain sharp bounds for the local stability of the defect-free state and to analyze the behavior of the new "spiral-like" state which emerges when the defect-free state loses stability. The spiral-like solution is always preferred to the defect-free state when it exists. In the weak anchoring scenario, we numerically compute stability diagrams (see Fig. 4) that quantify the sensitivity of the defect-free state to different kinds of perturbations in terms of the annular aspect ratio ρ, the elastic anisotropy δ and the anchoring strength α.

We model OF nematic equilibria with boundary defects by computing local solutions of the Laplace equation on an annular sector with Dirichlet tangent boundary conditions. We find three rotated and one diagonal solution, by analogy with similar work done for squares and rectangles in [15, 16, 21]. We compute analytic expressions for the corresponding director fields and their one-constant OF energy, and these expressions allow us to give qualitative information about the optimal number and arrangement of boundary defects, as a function of the annular aspect ratio. We note that the lowest energy states, made up of combinations of the U_2 sector configuration, are qualitatively similar to the experimentally observed states.

We study the conditions under which boundary defects may be energetically preferable to the defect-free state. Generically, we find that states with defects are preferred when the inner radius ρ is sufficiently small, the elastic anisotropy δ is sufficiently large, and the anchoring strength α is sufficiently small. These theoretical results are in qualitative agreement with experimental observations [4]. Although we consider elastic anisotropy and weak anchoring separately, we would expect the qualitative trends identified in Figs. 10 and 11 to hold for systems with both anisotropy and weak anchoring.

We illustrate the usefulness of the sector construction by using glued-together sector solutions to define initial conditions for an idealized LdG solver. The LdG simulations suggest that for moderate values of ρ and α with $\delta = 0$ (isotropic materials), an initial condition with boundary defects converges to a metastable solution with the same number of approximate singularities pinned to the inner and outer boundaries. Indeed, the sector-based equilibria may be a useful tool for constructing LdG equilibria that support boundary defects, and future work will include the study of LdG equilibria with boundary defects, their local and global stability in 2D and 3D settings.

Acknowledgments

We thank Dr. Oliver Dammone for valuable discussions. AL is supported by the Engineering and Physical Sciences Research Council (EPSRC) studentship. AM is supported by an EPSRC Career Acceleration Fellowship EP/J001686/1 and EP/J001686/2, an OCCAM Visiting Fellowship and the Keble Advanced Studies Centre. This publication is partly based on work supported by Award No. KUK-C1-013-04, made by King Abdullah University of Science and Technology (KAUST). In compliance with EPSRC's open access initiative, the data in this paper are available from http://dx.doi.org/10.5287/bodleian:R59G8pEMv.

References

1. P. G. de Gennes and J. Prost, *The Physics of Liquid Crystals* (2nd ed.), International Series of Monographs on Physics, Oxford University Press, Oxford, 1998.
2. E. G. Virga, *Variational Theories for Liquid Crystals*, Vol. 8, Chapman & Hall, London, 1995.
3. D. Dunmur and T. Sluckin, *Soap, Science and Flat-Screen TVs: A History of Liquid Crystals*, Oxford University Press, Oxford, 2010.
4. O. J. Dammone, Confinement of colloidal liquid crystals, Ph.D. Thesis, University College, University of Oxford, 2013.

5. J. Alvarado, Biological polymers: Confined, bent, and driven, Ph.D. Thesis, VU University Amsterdam, 2013.
6. I. C. Gârlea, P. Mulder, J. Alvarado, O. Dammone, D. G. A. L. Aarts, M. P. Lettinga, G. H. Koenderink, and B. M. Mulder, Finite particle size drives defect-mediated domain structures in strongly confined colloidal liquid crystals, *Nat. Commun.* 7 (2016).
7. F. Bethuel, H. Brezis, B. D. Coleman, and F. Hélein, Bifurcation analysis of minimizing harmonic maps describing the equilibrium of nematic phases between cylinders, *Arch. Ration. Mech. Anal.* 118:149–168 (1992).
8. T.-W. Pan, Existence and multiplicity of radial solutions describing the equilibrium of nematic liquid crystals on annular domains, *J. Math. Anal. Appl.* 245:266–281 (2000).
9. P. J. Barratt and B. R. Duffy, Weak-anchoring effects on a Fréedericksz transition in an annulus, *Liq. Cryst.* 19: 57–63 (1995).
10. P. J. Barratt and B. R. Duffy, Fréedericksz transitions in nematic liquid crystals in annular geometries, *J. Phys. D Appl. Phys.* 29:1551 (1996).
11. P. J. Barratt and B. R. Duffy, The effect of splay-bend elasticity on Fréedericksz transitions in an annulus, *Liq. Cryst.* 26: 743–751 (1999).
12. P. Palffy-Muhoray, A. Sparavigna, and A. Strigazzi, Saddle-splay and mechanical instability in nematics confined to a cylindrical annular geometry, *Liq. Cryst.* 14: 1143–1151 (1993).
13. P. Biscari and E. G. Virga, Local stability of biaxial nematic phases between two cylinders, *Int. J. Nonlinear Mech.* 32: 337–351 (1997).
14. G. Bevilacqua and G. Napoli, Periodic splay-twist Fréedericksz transition for nematics confined between two concentric cylinders, *Phys. Rev. E* 81:031707 (2010).
15. A. J. Davidson and N. J. Mottram, Conformal mapping techniques for the modelling of liquid crystal devices, *Eur. J. Appl. Math.* 23: 99–119 (2012).
16. A. H. Lewis, I. Garlea, J. Alvarado, O. J. Dammone, P. D. Howell, A. Majumdar, B. M. Mulder, M. P. Lettinga, G. H. Koenderink, and D. G. A. L. Aarts, Colloidal liquid crystals in rectangular confinement: Theory and experiment, *Soft Matter* 10: 7865–7873 (2014).
17. L. Berlyand and K. Voss, Symmetry breaking in annular domains for a Ginzburg-Landau superconductivity model, IUTAM Symposium on Mechanical and Electromagnetic Waves in Structured Media, *Solid Mechanics and Its Applications*, Vol. 91 (pp. 189–200), Springer Netherlands, 2002, ISBN 978-0-7923-7038-3.
18. A. Rapini and A. Papoular, Distorsion d'une lamelle nématique sous champ magnétique conditions d'ancrage aux parois, *J. Phys. Colloq.* 30: 54–56 (1969).
19. L. Evans, *Partial Differential Equations*, *Graduate Studies in Mathematics*, American Mathematical Society, Providence, Rhode Island, 2010.
20. R. T. de Souza, J. C. Dias, R. S. Mendes, and L. R. Evangelista, Critical exponents for Fréedricksz transition in nematics between concentric cylinders, *Physica A* 389: 945–950 (2010).
21. C. Tsakonas, A. J. Davidson, C. V. Brown, and N. J. Mottram, Multistable alignment states in nematic liquid crystal filled wells, *Appl. Phys. Lett.* 90:111913 (2007).
22. I. W. Stewart, *The Static and Dynamic Continuum Theory of Liquid Crystals: A Mathematical Introduction*, Liquid Crystals Book Series, Taylor & Francis, London, 2004.
23. H. Kusumaatmaja and A. Majumdar, Free energy pathways of a multistable liquid crystal device, *Soft Matter* 11: 4809–4817 (2015).

24. C. Luo, A. Majumdar, and R. Erban, Multistability in planar liquid crystal wells, *Phys. Rev. E* 85: 061702 (2012).
25. M. Nobili and G. Durand, Disorientation-induced disordering at a nematic-liquid-crystal–solid interface, *Phys. Rev. A* 46: R6174(R) (1992).

University of Oxford
University of Bath

(Received August 18, 2016)